The Cryosphere Discuss., 5, 2605–2628, 2011
www.the-cryosphere-discuss.net/5/2605/2011/
doi:10.5194/tcd-5-2605-2011

The Cryosphere Discussions

A numerical model for meltwater channel evolution in glaciers

A. H. Jarosch[1] **and M. T. Gudmundsson**[2]

[1]Centre for Climate and Cryosphere, Institute of Meteorology and Geophysics, University of Innsbruck, Innsbruck, Austria
[2]Institute of Earth Sciences, University of Iceland, Reykjavík, Iceland

Received: 23 September 2011 – Accepted: 3 October 2011 – Published: 11 October 2011

Correspondence to: A. H. Jarosch (alexander.jarosch@uibk.ac.at)

Published by Copernicus Publications on behalf of the European Geosciences Union.

Abstract

Meltwater channels form an integral part of the hydrological system of a glacier. Better understanding of how meltwater channels develop and evolve is required to fully comprehend supraglacial and englacial meltwater drainage. Incision of supraglacial stream channels and subsequent roof closure by ice deformation has been proposed in recent literature as a possible englacial conduit formation process. Field evidence for supraglacial stream incision has been found in Svalbard and Nepal. In Iceland, where volcanic activity provides meltwater with temperatures above 0 °C, rapid enlargement of supraglacial channels has been observed. By coupling, for the first time, a numerical ice dynamic model to a hydraulic model which includes heat transfer, we investigate the evolution of meltwater channels and their incision behaviour. We present results for different, constant meltwater fluxes, different channel slopes, different meltwater temperatures as well as temporal variations in meltwater flux. The key parameters governing incision rate and depth are the channel slope and the meltwater temperature loss to the ice. Meltwater flux controls channel width and to a lesser degree incision behaviour. Calculated Nusselt numbers suggest that turbulent forced convection is the main heat transfer mechanism in the studied meltwater channels.

1 Introduction

Flow of water through glaciers has received considerable attention from the scientific community since theoretical treatment of the phenomena began with two publications in 1972 (Röthlisberger, 1972; Shreve, 1972). Recently, two detailed review articles have summarized the current state of knowledge, one focusing on jökulhlaups (Björnsson, 2010), also known as glacial outburst floods, and the other focusing on Röthlisberger channels (Walder, 2010), which are water-filled, pressurized englacial channels.

TCD
5, 2605–2628, 2011

The formation and evolution of surface meltwater channels has been studied in the field (e.g., Knighton, 1981; Marston, 1983) as well as in the laboratory (e.g., Isenko et al., 2005) and treated analytically, as evolving from surface crevasses (e.g., Fountain and Walder, 1998) or forming during drainage of surface lakes (e.g., Raymond and Nolan, 2000). Supraglacial channels evolving into englacial conduits have been considered as a mechanism for the formation of englacial passages (e.g., Fountain and Walder, 1998; Benn et al., 2009; Gulley et al., 2009). The role of supraglacial drainage systems during englacial tuya eruptions is still not fully understood, but they are thought to play an important role as a controlling mechanism for eruption site lake levels (e.g., Smellie, 2006).

Simulating temporal and spatial evolution of meltwater channels in ice, which is key to understand the processes involved, requires adequate numerical models capable of resolving the underlying physics in great detail. Many studies focusing on water propagation in glaciers would benefit from a temporally as well as spatially resolved model, which facilitates investigation of the transient behaviour of such systems.

In this contribution we present a new model that for the first time provides explicit numerical simulation of meltwater channels with a focus on their evolution as well as their incision behaviour. We introduce the physical basis of our model in Sect. 2, followed by notes on the numerical implementation in Sect. 3. Subsequently we present model results for different key model parameters in Sect. 4 and close with conclusions and an outlook on future research.

2 Model physics

Our model consists of three components: (1) ice dynamics, (2) turbulent meltwater flow in open channels, and (3) thermal transfer between meltwater and ice. Figure 1 displays the principal geometry of our model setup and introduces several model parameters.

TCD
5, 2605–2628, 2011

Along the contact area between meltwater in an open channel and ice, which forms the channel geometry, heat exchange plays a key role in the evolution of the system. Within the scope of this paper, we focus on a specific interaction along this boundary: outward growth of the channel geometry driven by thermal melting of the ice walls, counteracted by creep closure of the same channel.

To successfully model the evolution of such a system, all three aforementioned components have to be combined, which mathematically form a Stefan problem (Lamé and Clapeyron, 1831; Stefan, 1891). We will first introduce the physics we use for each component and subsequently describe the numerical details in Sect. 3.

2.1 Ice dynamics

Ice is simulated as a Stokes fluid with a non-linear viscous behaviour. Starting with the Stokes equations

$$-\eta\nabla^2\boldsymbol{u} + \nabla p = \rho_{\text{ice}}\boldsymbol{g}, \tag{1}$$

$$\nabla\cdot\boldsymbol{u} = 0, \tag{2}$$

for which $\boldsymbol{u}$ denotes the velocity vector, p the pressure field, ρ_{ice} the ice density, and $\boldsymbol{g}$ the gravity vector, we further include the standard rheology of ice (Glen, 1955; Nye, 1957) in our physical representation, which leads to a non-linear ice viscosity such that

$$\eta = \frac{1}{2}A^{-\frac{1}{n}}\dot{\epsilon}^{\frac{1-n}{n}}. \tag{3}$$

Here we write the Glen rate factor as A, the Glen exponent as n and the effective strain rate as $\dot{\epsilon} = \sqrt{1/2\,\dot{\epsilon}_{ij}\dot{\epsilon}_{ji}}$. An obvious name for this physical description of ice would be a "Stokes–Glen" fluid, but it is more commonly referred to as a "Full Stokes" model.

TCD
5, 2605–2628, 2011

2.2 Open channel hydraulics

To simulate the turbulent flow of water in an open channel, we use the Gauckler–Manning formula (Gauckler, 1867; Manning, 1891), which relates cross-sectional, average velocity (V) in an open channel to its slope (β) and hydraulic radius (R_h). Although this is an empirical formula, it can be derived analytically from the phenomenological theory of turbulence (Gioia and Bombardelli, 2002). Based on the Gauckler–Manning formula, the water flux (Q) in an open channel can be expressed as

$$Q = VA_c = \frac{1}{n_c} R_h^{\frac{2}{3}} \beta^{\frac{1}{2}} A_c. \quad (4)$$

Here n_c is the Gauckler–Manning coefficient and the hydraulic radius can be written as $R_h = A_c/P$, with A_c the cross-sectional area of the flow and P the wetted perimeter.

2.3 Water – ice thermal transfer

Following the approach of Raymond and Nolan (2000), we can relate the melting at the channel walls to the energy loss in the water flow:

$$\rho_{ice} L \frac{dA_c}{dt} = \left(\rho_w C_w \frac{d\theta}{ds} + \rho_w g \beta \right) Q = \rho_w g(\beta + \gamma) Q \quad (5)$$

with L the latent heat of fusion per unit mass, ρ_w the water density, and C_w the heat capacity of water per unit mass. $d\theta/ds$ is the change in water temperature θ per unit length s along the channel. To simplify Eq. (5), we introduce in accordance with Raymond and Nolan (2000)

$$\gamma = \frac{C_w \frac{d\theta}{ds}}{g} \approx \frac{C_w \Delta\theta}{gl} \quad (6)$$

and assume $d\theta/ds$ to be the input from the water temperature above freezing $\Delta\theta$ divided by the distance l along the channel over which the temperature drops to freezing.

TCD
5, 2605–2628, 2011

To estimate the change in channel geometry normal to the wall (r_n) caused by melting, we use Eq. (4) to rewrite Eq. (5) such that

$$\frac{dA_c}{dt} = \frac{dr_n}{dt} P = \frac{\rho_w g(\beta+\gamma)Q}{\rho_{ice} L}. \quad (7)$$

2.4 Analytical maximum depth

For the previously defined moving boundary problem, one can compute a steady-state solution in which the radial melting is exactly in balance with the creep closure. By assuming a fixed, semi-circular geometry at the melting front, Fountain and Walder (1998) calculated a maximum penetration depth (D_{MAX}) of the channel for such a steady state as

$$D_{MAX} = \left(\frac{n\tilde{A}}{\rho_{ice} g}\right)\left[\left(\frac{\rho_w g}{2\pi\rho_{ice} L}\right)\left(\frac{\pi}{2n_c}\right)^{\frac{3}{4}} Q^{\frac{1}{4}} \beta^{\frac{11}{8}}\right]^{\frac{1}{n}}. \quad (8)$$

Note the usage of Nye's old rate factor convention here with $\tilde{A} = A^{-n}$ and that we set $u_e = 0$, which is the vertical ice velocity in Fountain and Walder (1998). We will compare results computed with Eq. (8) with our numerical model results later in Sect. 4.

3 Numerical implementation

3.1 Stokes–Glen fluid

The non-linear Stokes–Glen fluid described by Eqs. (1–3) can be easily solved for complex geometries using the finite element method (FEM, e.g., Zienkiewicz et al., 2005). We use *icetools* (Jarosch, 2008) in its revised version[1] to solve the ice dynamics for our transient complex geometries. To achieve convergence of the non-linear viscosity

[1] http://icetools.sourceforge.net (ver.: 0.9)

TCD
5, 2605–2628, 2011

problem we substitute successively $\boldsymbol{u}$ and η in a classical Picard iteration. Further details on the numerical implementation, e.g. how we handle Eq. (3) in case of vanishing strain rate, can be found in Jarosch (2008).

3.2 Ice geometry and boundaries

We embed the evolving meltwater channel into a rectangular, two dimensional cross-section (along the x and z coordinate) of an idealized glacier. The point of origin for our model coordinate system is at the base in the centre of the glacier cross-section. Any forming meltwater channel is located at $x = 0$ m and at the initial glacier surface, where a predefined small surface depression facilitates the initial location of the meltwater stream (cf. Fig. 3a). In the model it is possible for the glacier surface to slope perpendicular towards the channel by setting the slope angle $\alpha > 0$ (cf. Fig. 1). We set $\boldsymbol{u} = 0$ at the lateral ice boundaries as well as at the basal boundary. To avoid any influence from these static boundaries on the evolving channel, we move the lateral boundaries to $x = \pm 1900$ m and set the initial ice surface at $z = 500$ m. The ice surface, including the meltwater channel wall, is modelled as a stress free boundary and we use a forward Euler scheme on the same grid to evolve the surface for each time step (cf. Jarosch, 2008). For the sake of simplicity and to purely focus on the meltwater channel evolution, we disregard surface mass balance for all model results in this paper. Considering the placement of our coordinate system, we could impose a symmetry boundary at $x = 0$ m to simplify the model and only simulate one half-space of the domain. As a test for the numerical stability of our model, we choose to do otherwise and model the full domain for which we only impose an initially symmetric geometry. As we will later demonstrate (cf. Fig. 4), the transient simulations stay almost perfectly symmetric over long time spans.

The interface between meltwater and ice (red line in Figs. 1 and 2a) demands closer attention, as there are several physical processes (cf. Sects. 2.2 and 2.3) involved in the temporal evolution of this boundary. In the next section we describe in detail how the

TCD
5, 2605–2628, 2011

interaction between ice dynamics, channel hydraulics and wall melting is implemented numerically.

3.3 Moving channel boundary

At each time step of the evolving model, we have to account for all three aforementioned processes. If we would model the turbulent water flow in the channel explicitly within the FEM model, we could use an iterative scheme commonly used in fluid structure interaction models (e.g., Bungartz, 2010) to simulate the moving boundary. Here we choose a much simpler approach as we model heat transfer from meltwater to ice with Eq. (7) and meltwater hydraulics with Eq. (4). Figure 2 illustrates our two step scheme to move the boundary forward at each time step.

First, we estimate P and A_c for a given flux Q by inverting Eq. (4) and making use of the known channel geometry. Equation (7) can be used to calculate the area change of the channel tip caused by melting. To distribute dr_n along P, we scale dr_n with the maximal water height (H_{max}) inside the channel (cf. Fig. 2a) to achieve maximal melt at the deepest part. This is a similar yet somewhat less constraining approach to the one of Fountain and Walder (1998), where they distribute dr_n as a function of angle along P, effectively scaling it with the angle from vertical and thus prescribing a circular geometry at the channel tip. We, on the other hand, do not prescribe any channel geometry nor the location of the deepest part (H_{max}), which enables the model to evolve the channel shape during a simulation. By combining all these estimates, we can now move the boundary grid points outward, by using the model's time step Δt and a forward Euler scheme, to simulate the geometry change due to melting (cf. Fig. 2a).

Second, ice deformation will counteract the expansion of the channel. We make use of surface velocities from the ice dynamics model, which is solved using the geometry established in the first step (cf. Fig. 2a), and Δt to move all surface points, including the grid points inside the channel (cf. Fig. 2b). In this step, the surface is considered stress free and the water body inside the channel is ignored.

TCD
5, 2605–2628, 2011

Finally, the new channel geometry is established for the model time $t_{i+1} = t_i + \Delta t$ (cf. Fig. 2c). Δt can be chosen to be either fixed at a value small enough to avoid numerical instabilities or by utilizing a CFL condition (e.g., Courant et al., 1928) on the forward moving grid, which calculates an optimal value for Δt. As the surface grid points move at each time step, we also regenerate the numerical mesh for the FEM model using the updated geometry. Figure 3 displays the evolution of a typical channel in our model. In this example, a predefined flux of $Q = 1\,\mathrm{m}^3\,\mathrm{s}^{-1}$ is used to fill an initial, small surface depression and subsequently the model evolves over 20 days ($\Delta t = 2$ days) to form a meltwater channel. Note that the channel width changes over time (Fig. 3a–c) and the channel width after 20 days (Fig. 3c) is a result of the model physics and not prescribed by us.

3.4 Channel pinch-off and flow regime transition

After a certain time (t_p) of model evolution, the channel is pinched off from the surface due to ice deformation. At this stage, the numerical mesh along the ice walls in the channel merges above the channel bottom (cf. Fig. 4). The closure velocity of the channel walls at that location decreases to zero as the mesh re-merges, simulating a direct contact and instant refreezing of the channel walls. Numerically, a control algorithm monitors the grid points at the channel walls and detects overlaps, for which the numerical mesh is merged at these locations.

As time progresses, ice flow continues to act on the channel geometry and the channel's cross-sectional area decreases until it is sufficiently small to fill the whole channel with meltwater. At this timestep (t_final), Eq. (4) is not valid anymore and the channel hydraulics switch to a pressurized channel flow. In pressurized channels, radial melting is balanced by radial inward creep of ice, thus no significant downward motion is to be expected (e.g., Röthlisberger, 1972). We discuss possible extensions of the model to include pressurized channel flow in Sect. 5.

TCD
5, 2605–2628, 2011

4 Results

In this section we investigate the behavior of the presented model for different model parameters. Obviously there exists a large model parameter space, which could be explored, but we will focus here on a small sub-set, which is intended to demonstrate the general behaviour of the model.

For all results presented here, we set several model parameters to fixed values, which are listed in Table 1. Moreover, we keep the initial ice geometry with its boundary conditions predefined (cf. Sect. 3.2 and Fig. 3a) except the ice surface slope angle α. The meltwater temperature within the channel is assumed to be zero for most results, which leads to $d\theta/ds = 0\,^{\circ}\mathrm{C\,m^{-1}}$ and therefore $\gamma = 0$. An increase of meltwater temperature provides more energy to melt ice, but does not change the general behaviour of the model. Note that the contribution of either channel slope (β) or meltwater temperature gradient factor (γ) to cross-sectional area change (dA_c/dt) is linear in Eqs. (5) and (7), and thus it is sufficient to vary one for a demonstration of model behaviour. For example, increasing the channel slope (β) by 0.03 is equivalent to $\Delta T \approx 0.35\,^{\circ}\mathrm{C}$ over a channel distance $l = 5000\,\mathrm{m}$, or $d\theta/ds = 7 \times 10^{-5}\,^{\circ}\mathrm{C\,m^{-1}}$.

4.1 Constant meltwater flux

In Fig. 5, we present results for several meltwater fluxes Q, glacier surface slopes α, channel slopes β, and meltwater temperature loss along the channel $d\theta/ds$. All simulations are computed until t_{final} is reached, except for the $Q = 0.1\,\mathrm{m^3\,s^{-1}}$, $\beta = 0.03$ and the $Q = 1\,\mathrm{m^3\,s^{-1}}$, $\beta = 0.01$ run. Those two runs are stopped after 4000 days, as their incision rate is very low.

Shades of blue mark results for $Q = 1\,\mathrm{m^3\,s^{-1}}$ and varying slope parameters (α and β) in Fig. 5. We define the reference run for $\alpha = 0.0$ and $\beta = 0.03$ (cf. thick blue line in Fig. 5). By comparing our numerical reference run with the analytical maximum depth for the same parameter set computed with Eq. (8), we find that the transient simulation estimates a considerably shallower maximum incision (159 m less, cf. Fig. 5

TCD
5, 2605–2628, 2011

and Table 2). This clearly demonstrates that the temporal evolution of the channel is playing a key role in the simulation as well as the flow regime switch at the end, which both effectively limit the incision behaviour.

Increasing the glacier surface slope (α) in the reference run results in an increased ice flow towards the channel, and thus a shallower incision depth (12 m less at t_{final}, cf. Fig. 5 and Table 2). Also the channel pinch-off t_p occurs earlier ($t_p = 280$ vs. $t_p = 366$ days). Doubling the channel slope (β), on the other hand, leads to increased downward melting and thus a deeper incision depth (43 m more at t_{final}, cf. Fig. 5 and Table 2). Again the channel pinch-off t_p occurs earlier ($t_p = 190$ vs. $t_p = 366$ days) in comparison with the reference run. A similar result can be achieved by increasing the meltwater flux by one order of magnitude to $Q = 10\,m^3\,s^{-1}$ (cf. red line in Fig. 5). An increased meltwater flux produces a wider channel ($w_c = 1.12$ m vs. $w_c = 0.63$ m, cf. Table 2), which requires significantly more melting to create a similar incision behaviour as the $Q = 1\,m^3\,s^{-1}$ and $\beta = 0.06$ case. Note that in this case the incision depth is shallower (29 m less at t_{final}, cf. Fig. 5 and Table 2). Decreasing the channel slope to $\beta = 0.01$, but keeping the meltwater flux at $Q = 10\,m^3\,s^{-1}$ results in a similar behaviour as the reference run, but with a much shallower incision depth (31 m less at t_{final}, cf. Fig. 5 and Table 2) and a later pinch-off ($t_p = 408$ vs. $t_p = 366$ days).

For comparison, we decrease the meltwater flux by one order of magnitude from the reference run to $Q = 0.1\,m^3\,s^{-1}$ (cf. black line in Fig. 5), which causes a very slow incision rate. We can achieve a similar incision rate by keeping the meltwater flux at $Q = 1.0\,m^3\,s^{-1}$, but decreasing the channel slope to $\beta = 0.01$.

To complete our results for constant meltwater fluxes, we include two extreme cases in Fig. 5. A meltwater flux of $Q = 100\,m^3\,s^{-1}$ leads to a rapid incision rate, but not to a significantly deeper incision in comparison to the same model setup with $Q = 10\,m^3\,s^{-1}$. At $t_{final} = 398$ days the channel with $Q = 100\,m^3\,s^{-1}$ reached a depth of 112 m, whereas the channel with $Q = 10\,m^3 s^{-1}$ requires 1276 days (t_{final}) to reach a depth of 90 m (cf. Fig. 5 and Table 2).

TCD
5, 2605–2628, 2011

The second extreme case introduces a meltwater temperature loss of $d\theta/ds = 0.002\,^{\circ}\mathrm{C\,m^{-1}}$ at a flux $Q = 10\,\mathrm{m^3\,s^{-1}}$. This meltwater temperature change along the channel corresponds to the values found in the 1996 Gjálp eruption, Vatnajökull ice cap, Iceland (based on Fig. 8 and Table 3 in Gudmundsson et al., 2004). Such a scenario provides a large amount of energy to melt ice within the channel, which leads to an incision of 379 m over 60.45 days[2] (cf. Fig. 5 and Table 2).

More information on the mechanism of heat transfer at the water-ice boundary can be obtained by calculating the Nusselt number Nu for each model setup. In Table 2, we present Nusselt numbers for a forced turbulent flow regime based on the work of Lunardini et al. (1986), which is valid for Reynolds numbers $Re > 1.5-2\times10^4$. We find $Nu > 1000$ for all presented simulations, which indicates that turbulent forced convection is the main heat transfer mechanism.

Clearly β as well as $d\theta/ds$ (and thus γ) can be identified as the most sensitive model parameters with respect to incision depth and rate. A twofold increase in β results in a faster incision rate than an order of magnitude increase in Q. On the other hand, reducing β to one third leads to a similar incision rate as obtained by an order of magnitude decrease in Q. Comparing our reference run with the analytical maximum depth for the same parameter set demonstrates the importance of simulating the transient behaviour of the system.

4.2 Variable meltwater flux

To simulate an idealized meltwater flux cycle throughout a year, we vary Q over time such that

$$Q(t) = \max\left[Q_{\max}\sin\left(\frac{2\pi t\,\Delta t}{365}\right), 0\right], \tag{9}$$

which results in a period of half a year in which Q increases to $Q_{\max}$ and decreases again to zero as well as half a year period with no meltwater flux. This is intended to

[2]This simulation uses $\Delta t = 0.05$ days and thus such a high accuracy in time is given.

TCD
5, 2605–2628, 2011

represent more realistic meltwater runoff conditions on glaciers. We use the same sets of model parameters as in Fig. 5 for $Q = 1\,m^3\,s^{-1}$ and $\beta = 0.03$, 0.06 (shades of blue), but now we set $Q_{max} = 1\,m^3\,s^{-1}$ and use Eq. (9) to vary Q with time. Results of these simulations are displayed in Fig. 6.

Similar results as for constant meltwater fluxes can be observed. Again a twofold increase in β leads to a deeper incision (13 m more at $t = 182.5$ days) and increased ice flow towards the channel ($\alpha > 0$) counteracts the channel evolution. The pronounced difference to the constant meltwater flux case is the period of no incision during which $Q = 0\,m^3\,s^{-1}$. In the case of increased ice flow towards the channel, the channel bottom even rises again during this period (cf. light blue line in Fig. 6).

5 Conclusions and outlook

In this paper we have presented a new model that for the first time provides explicit numerical simulation of meltwater channel evolution in glaciers, based on the combination of ice dynamics, open channel hydraulics, and ice-water thermal transfer. The model is capable of simulating channel incision over time for a given meltwater flux, meltwater temperature, channel slope, and initial ice geometry. Shape and evolution of the channel are purely driven by model physics and are not pre-defined.

To demonstrate the principal model behaviour, we have computed solutions for a set of model parameters. In case of constant meltwater fluxes, we have identified the channel slope β as well as the meltwater temperature loss to ice $d\theta/ds$ (γ) to be the main controlling parameters for channel incision depth and rate. Smaller channel slopes lead to wider channels. Q mainly controls channel width and to a lesser degree channel incision rate. Increased ice flow towards the channel ($\alpha > 0$) counteracts channel incision. Comparison with a steady-state estimation of maximum incision depth clearly demonstrates the importance of resolving the transient nature of the system. Calculated Nusselt numbers suggest that turbulent forced convection is the main heat transfer mechanism in the studied meltwater channels.

TCD
5, 2605–2628, 2011

We have also computed results for Q varying over a synthetic annual cycle, creating a half year period of increase and subsequent decrease followed by a half year period of no water flux. Similar model behaviour can be observed. Again β is the most important model parameter with respect to incision depth. The period of $Q = 0\,\mathrm{m}^3\,\mathrm{s}^{-1}$ shows no downward motion of the channel bottom and can be considered to be representative of wintertime conditions. In the case of $\alpha > 0$, ice deformation not only counteracts the incision process, but causes an uplift of the channel bottom during the winter regime.

Currently the model is limited to simulate cases of open channel flow. A possible future expansion of the model would be to simulate the meltwater flow within the channel explicitly in a FEM simulation and couple it to the existing model. This would not only allow for a transition from open to pressurized channel flow, but would also enable an explicit simulation of heat transfer processes on the water-ice boundary, which is crucial for the treatment of cold ice conditions. The simulation of fully developed turbulent water flow in channels and pipes is a numerically complex and difficult task, especially in the case of free surface flow, so this model extension remains a challenge for future research.

Because the presented model is capable of simulating meltwater channel evolution dynamically, based on a state of the art ice dynamics model, we foresee that this approach holds great promise for glacier-hydrological modelling applied to jökulhlaup evolution, moulin formation and evolution, surface lake drainage, and even englacial ice-volcano interaction.

Acknowledgements. We would like to thank G. E. Flowers for stimulating discussions and L. Nicholson, M. Hofer, and R. Prinz for helping to improve the clarity of the manuscript. Financial support for this project has been provided by the University of Iceland Research Fund and the Austrian Science Fund (FWF): P22106-N21.

TCD
5, 2605–2628, 2011

References

Benn, D., Gulley, J., Luckman, A., Adamek, A., and Glowacki, P. S.: Englacial drainage systems formed by hydrologically driven crevasse propagation, J. Glaciol., 55, 513–523, 2009. 2607

Björnsson, H.: Understanding jökulhlaups: from tale to theory, J. Glaciol., 56, 1002–1010, 2010. 2606

Bungartz, H. J.: Fluid Structure Interaction II: Modelling, Simulation, Optimization, Lecture Notes in Computational Science and Engineering, Springer, Berlin Heidelberg, Germany, 2010. 2612

Courant, R., Friedrichs, K., and Lewy, H.: Über die partiellen Differenzengleichungen der mathematischen Physik, Math. Ann., 100, 32–74, 1928. 2613

Cuffey, K. M. and Paterson, W. S. B.: The Physics of Glaciers, Elsevier Butterworth-Heinemann, 4 Edn., Burlington, USA, 2010. 2621

Fountain, A. G. and Walder, J. S.: Water flow through temperate glaciers, Rev. Geophys., 36, 299–328, 1998. 2607, 2610, 2612, 2621

Gauckler, P. G.: Etudes Théoriques et Pratiques sur l'Ecoulement et le Mouvement des Eaux, Tech. rep., Comptes Rendues de l'Académie des Sciences, Paris, France, 1867. 2609

Gioia, G. and Bombardelli, F. A.: Scaling and similarity in rough channel flows, Phys. Rev. Lett., 88, 1–4, doi:10.1103/PhysRevLett.88.014501, 2002. 2609

Glen, J. W.: The creep of polycrystalline ice, P. Roy. Soc. A-Math. Phy., 228, 519–538, doi:10.1098/rspa.1955.0066, 1955. 2608

Gudmundsson, M. T., Sigmundsson, F., Björnsson, H., and Högnadóttir, T.: The 1996 eruption at Gjálp, Vatnajökull ice cap, Iceland: efficiency of heat transfer, ice deformation and subglacial water pressure, B. Volcanol., 66, 46–65, doi:10.1007/s00445-003-0295-9, 2004. 2616

Gulley, J., Benn, D., Müller, D., and Luckman, A.: A cut-and-closure origin for englacial conduits in uncrevassed regions of polythermal glaciers, J. Glaciol., 55, 66–80, doi:10.3189/002214309788608930, 2009. 2607

Isenko, E., Naruse, R., and Mavlyudov, B.: Water temperature in englacial and supraglacial channels: change along the flow and contribution to ice melting on the channel wall, Cold Reg. Sci. Technol., 42, 53–62, doi:10.1016/j.coldregions.2004.12.003, 2005. 2607

Jarosch, A. H.: Icetools: a full Stokes finite element model for glaciers, Comput. Geosci., 34, 1005–1014, doi:10.1016/j.cageo.2007.06.012, 2008. 2610, 2611

TCD
5, 2605–2628, 2011

Knighton, A. D.: Channel form and flow characteristics of supraglacial streams, Austre Okstindbreen, Norway, Arctic Alpine Res., 13, 295–306, 1981. 2607
Lamé, G. and Clapeyron, B. D.: Mémoire sur la solidification par refroidissement d'un globe liquide, Ann. Chim. Phys., 47, 250–256, 1831. 2608
Lunardini, V. J., Zisson, J. R., and Yen, Y. C.: Experimental determination of heat transfer coefficients in water flowing over a horizontal ice sheet, Tech. rep., Cold Region Research and Engineering Laboratory, Hanover, 1986. 2616
Manning, R.: On the flow of water in open channels and pipes, Transactions of the Institution of Civil Engineers of Ireland, ICE Transactions, 20, 161–207, 1891. 2609
Marston, R.: Supraglacial stream dynamics on the Juneau Icefield, Ann Assoc. Am. Geogr., 73, 597–608, 1983. 2607
Nye, J. F.: The distribution of stress and velocity in glaciers and ice-sheets, P. Roy. Soc. A-Math. Phy., 239, 113–133, 1957. 2608
Raymond, C. F. and Nolan, M.: Drainage of a glacial lake through an ice spillway, in: IAHS PUBLICATION, edited by: Nakawo, M., Raymond, C. F., and Fountain, A., no. 264 in IAHS Publication, International Association of Hydrological Sciences, 199–210, Washington, USA, 2000. 2607, 2609
Röthlisberger, H.: Water pressure in intra-and subglacial channels, J. Glaciol., 11, 177–203, 1972. 2606, 2613
Shreve, R.: Movement of water in glaciers, J. Glaciol., 11, 205–214, 1972. 2606
Smellie, J.: The relative importance of supraglacial versus subglacial meltwater escape in basaltic subglacial tuya eruptions: an important unresolved conundrum, Earth-Sci. Rev., 74, 241–268, doi:10.1016/j.earscirev.2005.09.004, 2006. 2607
Stefan, J.: Über die Theorie der Eisbildung, insbesondere über die Eisbildung in Polarmeere, Ann. Phys., 278, 269–286, doi:10.1002/andp.18912780206, 1891. 2608
Walder, J. S.: Röthlisberger channel theory: its origins and consequences, J. Glaciol., 56, 1079–1086, 2010. 2606
Zienkiewicz, O. C., Taylor, R. L., and Zhu, J. Z.: The finite element method: its basis and fundamentals, The Finite Element Method, Elsevier Butterworth-Heinemann, 6 Edn., Oxford, UK, 2005. 2610

TCD
5, 2605–2628, 2011

Table 1. Constants used in this manuscript. We assume temperate ice and take the corresponding value for A from Cuffey and Walder (2010, p. 75). n_c for ice channels is taken from Fountain and Walder (1998).

Symbol	Value
A	$2.4 \times 10^{-24}\,\mathrm{s^{-1}\,Pa^{-3}}$
n	3
n_c	$0.01\,\mathrm{s\,m^{-1/3}}$
ρ_{ice}	$900\,\mathrm{kg\,m^{-3}}$
ρ_w	$1000\,\mathrm{kg\,m^{-3}}$
g	$9.8\,\mathrm{m\,s^{-2}}$
L	$3.35 \times 10^5\,\mathrm{J\,kg^{-1}}$
C_w	$4210\,\mathrm{J\,kg^{-1}\,K^{-1}}$

TCD
5, 2605–2628, 2011

Table 2. Tabular form of results displayed in Fig. 5. Height of the channel bottom above point of origin is denoted with h_c, whereas d_c is the depth of the channel measured from the initial surface. Both incision measures are for model time t_{final}, at which the channel switches from an open channel flow regime to a pressurized channel, while at t_p the channel pinch-off occurs. Channel width w_c is measured as the widest part of the moving channel tip passes $z = 480$ m. Nu are Nusselt numbers and Re the Reynolds numbers. Values for our reference run are bold.

Q $m^3\,s^{-1}$	α deg	β rad	$d\theta/ds$ $K\,m^{-1}$	h_c m	d_c m	t_{final} days	t_p days	w_c m	Nu $\times 10^3$	Re $\times 10^6$
0.1	0.0	0.03	0.0	–	–	–	944	0.27	1.25	0.16
1.0	0.0	0.01	0.0	–	–	–	1080	0.80	3.97	0.57
1.0	**0.0**	**0.03**	**0.0**	**379**	**121**	**1962**	**366**	**0.66**	**4.77**	**0.70**
1.0	1.0	0.03	0.0	391	109	1882	280	0.65	4.77	0.70
1.0	0.0	0.06	0.0	336	164	1147	190	0.63	5.38	0.80
10.0	0.0	0.01	0.0	410	90	1276	408	1.97	14.91	2.39
10.0	0.0	0.03	0.0	365	135	1090	278	1.12	16.59	2.68
10.0	0.0	0.01	0.002	121	379	60.45	11.45	1.83	14.75	2.36
100.0	0.0	0.01	0.0	388	112	398	152	4.52	55.55	9.88

TCD
5, 2605–2628, 2011

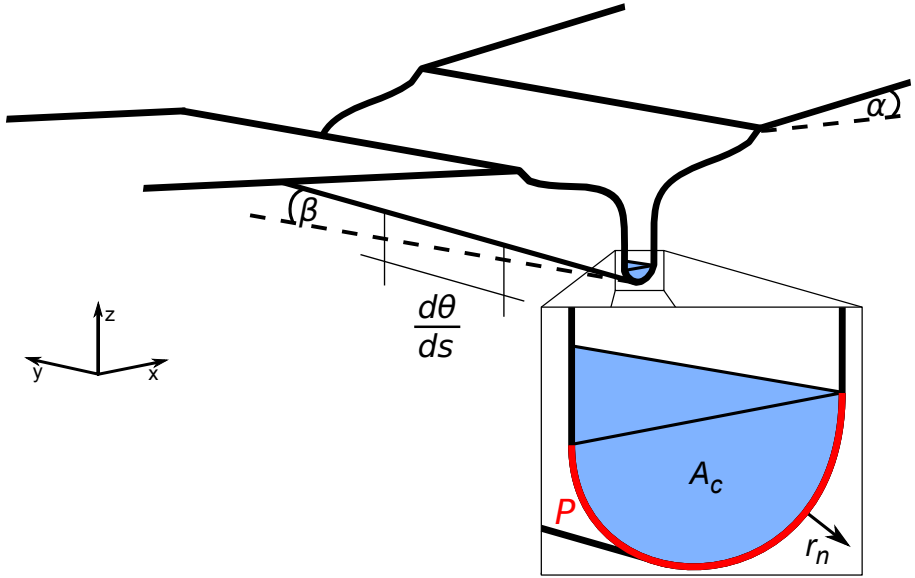

Fig. 1. Sketch of the model geometry which indicates several model parameters as defined in Sects. 2 and 3.

TCD
5, 2605–2628, 2011

Meltwater channel model

A. H. Jarosch and
M. T. Gudmundsson

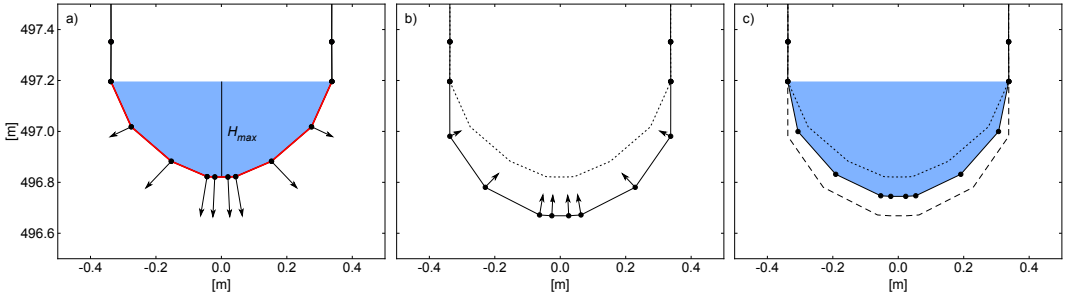

Fig. 2. Forward stepping scheme for the moving melt boundary at each time step. In **(a)**, melt processes expand the channel below the water level along the wetted perimeter (red line). Subsequently ice deformation closes the channel **(b)**, which leads to the final geometry at this time step **(c)**. The dotted line marks the channel shape from the prior time step, the dashed line the intermediate geometry after melt, and H_{max} denotes the maximal water height inside the channel. Please note that ice deformation is greatly enhanced in **(b)** and neglected above the water line in this sketch to facilitate clarity.

TCD
5, 2605–2628, 2011

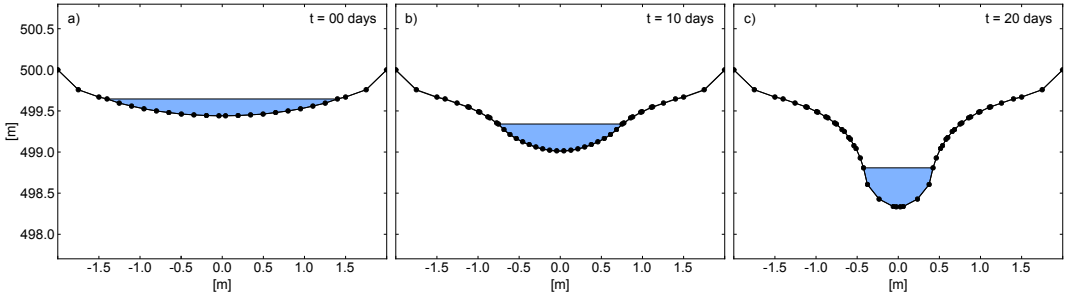

Fig. 3. Evolution of the meltwater channel for $t = 0$ days **(a)**, $t = 10$ days **(b)**, and $t = 20$ days **(c)** with $Q = 1\,\mathrm{m}^3\,\mathrm{s}^{-1}$, $\alpha = 0.0$, $\beta = 0.03$ and $d\theta/ds = 0\,^{\circ}\mathrm{C}\,\mathrm{m}^{-1}$.

TCD
5, 2605–2628, 2011

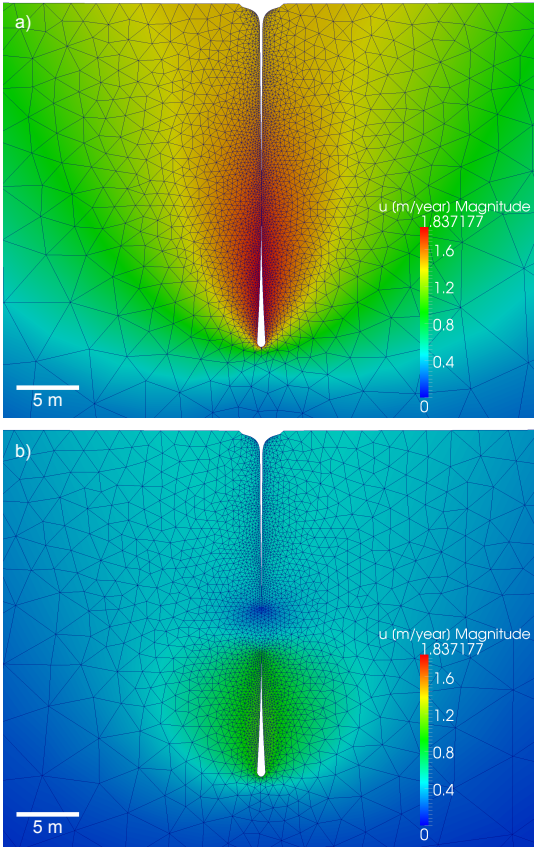

Fig. 4. Magnitude of velocity field for a simulation with $Q = 1\,\mathrm{m}^3\,\mathrm{s}^{-1}$, $d\theta/ds = 0\,^\circ\mathrm{C\,m}^{-1}$, $\alpha = 0.0$ and $\beta = 0.03$ at $t_\mathrm{p} = 366$ days **(a)** and $t = 368$ days **(b)**. Between the two presented time steps, the channel pinches off from the surface and in **(b)**, the numerical mesh already merged above the channel bottom.

TCD
5, 2605–2628, 2011

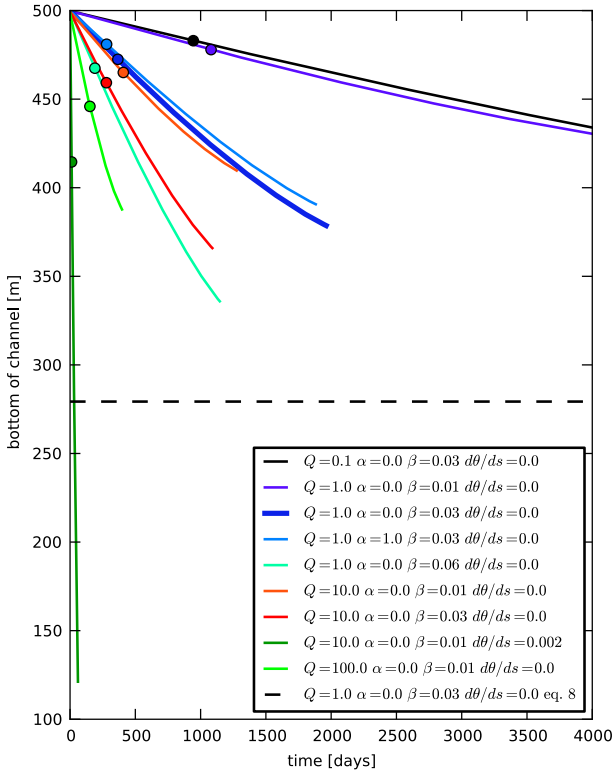

Fig. 5. Evolution of channel bottom with respect to point of origin for different meltwater fluxes Q, glacier surface slopes α, channel slopes β, and water temperature loss $d\theta/ds$ are plotted with different colors. The timestep (t_p) at which the channel pinches off is marked with a colored dot for each model. For $Q = 1\ m^3\ s^{-1}$ and $\alpha = 0.0$, the solution of Eq. (8) is displayed as a dashed line.

TCD
5, 2605–2628, 2011

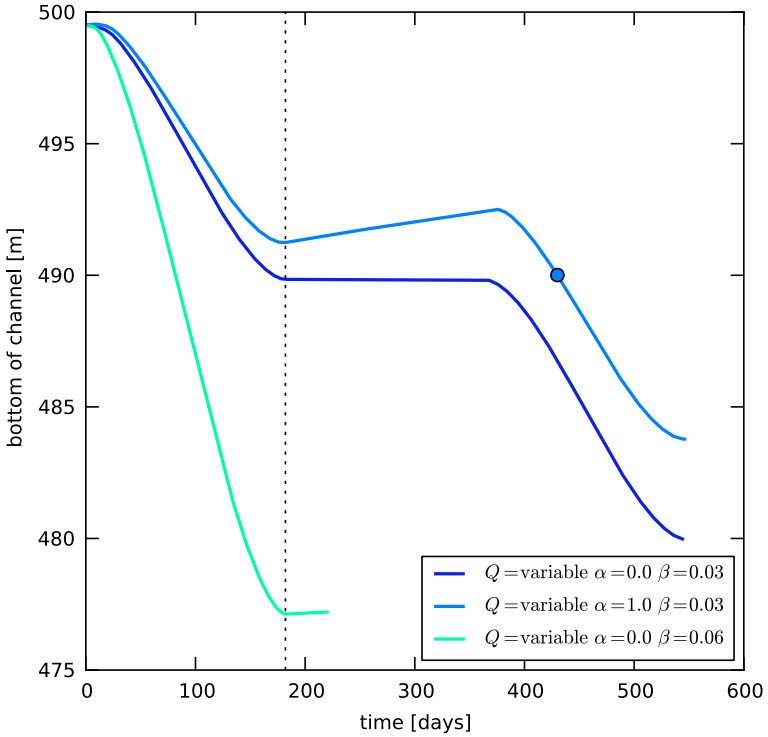

Fig. 6. Evolution of channel bottom with respect to point of origin for a time varying flux Q, different glacier surface slopes α, and different channel slopes β are plotted with different colors. The timestep (t_p) at which the channel pinches off is marked with a colored dot for one model, whereas in the other models, the channel does not pinch-off during the simulation. All solutions displayed here use $d\theta/ds = 0\,^{\circ}\mathrm{C\,m^{-1}}$. Model time $t = 182.5$ days, after which $Q(t) = 0\,\mathrm{m^3\,s^{-1}}$ for half a year, is marked with the vertical dashed line. For $\beta = 0.03$, we plot results for one and a half years to demonstrate a whole year's cycle and the subsequent period for which $Q > 0\,\mathrm{m^3\,s^{-1}}$. In the case of $\beta = 0.06$, we plot results to $t = 220$ days, highlighting the different model behaviour for the first half of a year.

TCD
5, 2605–2628, 2011